Labeling TiO$_2$ Nanoparticles with Dyes for Optical Fluorescence Microscopy and Determination of TiO$_2$-DNA Nanoconjugate Stability

Kenneth T. Thurn[1], **Tatjana Paunesku**[1], **Aiguo Wu**[1], **Eric M.B. Brown**[1], **Barry Lai**[2], **Stefan Vogt**[2], **Jörg Maser**[3], **Mohammed Aslam**[4], **Vinayak Dravid**[5], **Raymond Bergan**[6], and **Gayle Woloschak**[1,7,*]

[1]Department of Radiation Oncology, Northwestern University Feinberg School of Medicine Chicago, IL 60611

[2]X-Ray Science Division, Advanced Photon source, Argonne National Laboratory, Argonne, IL, 60439

[3]Center for Nanoscale Materials, Advanced Photon Source, Argonne National Laboratory, Argonne, IL 60439

[4]Department of Physics, Indian Institute of Technology Bombay Powai, Mumbai 400076, India

[5]Department of Material Science and Engineering, and NUANCE Center, Northwestern University, Evanston IL 60208

[6]Department of Medicine, Robert H. Lurie Cancer Center, Northwestern University Feinberg School of Medicine, Chicago, IL 60611

[7]Departments of Radiology, and Cell and Molecular Biology, Northwestern University Feinberg School of Medicine, Chicago, IL 60611

Abstract

Visualization of nanoparticles without intrinsic optical fluorescence properties is a significant problem when performing intracellular studies. Such is the case with titanium dioxide (TiO$_2$) nanoparticles. These nanoparticles, when electronically linked to single stranded DNA oligonucleotides, have been proposed to be used both as gene knockout devices and as possible tumor imaging agents. By interacting with complementary target sequences in living cells, these photo-inducible TiO$_2$-DNA nanoconjugates have the potential to cleave intracellular genomic DNA in a sequence specific and inducible manner. The nanoconjugates also become detectable by magnetic resonance imaging (MRI) with the addition of gadolinium Gd(III) contrast agents. Herein we describe two approaches for labeling TiO$_2$ nanoparticles and TiO$_2$-DNA nanoconjugates with optically fluorescent agents. This permits, for the first time, direct quantification of fluorescently labeled TiO$_2$ nanoparticle uptake in a large population of living cells ($>10^4$ cells). X-Ray Fluorescence Microscopy (XFM) was combined with fluorescent microscopy to determine the relative intracellular stability of the nanoconjugates. It was also used to quantify intracellular nanoparticles. Imaging the DNA component of the TiO$_2$-DNA nanoconjugate by fluorescent confocal microscopy within the same cell showed an overlap with the titanium signal as mapped by XFM. This strongly implies the intracellular integrity of the TiO$_2$-DNA nanoconjugates in malignant cells.

*Prof. Gayle Woloschak, 303 E. Chicago Ave., Ward Building Room 13-007, Chicago IL, 60611 (USA), g-woloschak@northwestern.edu.

Keywords

TiO$_2$-DNA Nanoconjugate; Nanoparticle; X-Ray Fluorescence Microscopy; Titanium Dioxide

1. Introduction

Some of the most examined nanoparticles to date are those composed of titanium dioxide (TiO$_2$) due to their unique photocatalytic and structural properties. TiO$_2$ nanoparticles have been investigated for potential uses as disinfectants,[1-3] diagnostic assays,[4] biological probes,[5] tumor cell killing agents,[6-8] and even for gene targeting.[9-11] These nanoparticles make an attractive mechanism to target cancer cells since photo-activation of TiO$_2$ (1000 μg/ml) with energies of 3.2 eV causes a release of reactive oxygen species (ROS). [12] Photo-excited TiO$_2$ nanoparticles were shown to cause significant cell death in various cancer cell lines.[6-8] While the bulk form of TiO$_2$ is considered generally biologically inert, [1] there is some controversy as to the extent of TiO$_2$ nanoparticle cytoxicity.[8,13-16] Recently, however, intravenous tail-vein injection of 5 mg/kg of TiO$_2$ nanoparticles (<100 nm) into male Wistar rats showed no deleterious effects on organ function and caused no detectable inflammatory response *in vivo*.[17]

Our laboratory is investigating the use of TiO$_2$ nanoparticles bound to single stranded DNA oligonucleotides creating TiO$_2$-DNA nanoconjugates. Reduction of particle size below 20 nm results in TiO$_2$ surface corner defects that can be repaired through covalent bonds with ortho-substituted enediol ligands (e.g. dopamine, alizarin) forming stable charge transfer complexes. [18-20] The TiO$_2$-DNA nanoconjugates are being examined as potential gene targeting devices, and imaging agents for the detection of tumors. The nanoconjugate consists of a TiO$_2$ nanoparticle covalently bound to dopamine which is itself bound to a single stranded DNA oligonucleotide (Figure 1).[9] The DNA maintains its sequence specific hybridization, while the nanoparticle component maintains its photocatalytic properties.[9,20] When photo-activated, a charge separation occurs within the nanoparticle, resulting in the migration of an electropositive hole (h$^+$) from the nanoparticle, through the dopamine, and onto the DNA[20, 21] finally resulting in its scission.[9] Therefore, TiO$_2$-DNA nanoconjugates should be able to specifically cleave mutated genomic DNA in a sequence-specific and inducible manner. In this way, they have the potential to specifically and effectively target oncogenes that represent desirable therapeutic targets (e.g. ras, myc).[22-25] By conjugating dopamine modified gadolinium Gd(III) contrast agents directly to the surface of the TiO$_2$ nanoparticle, the nanoconjugates become detectable by T$_1$ weighted Magnetic Resonance Imaging (MRI),[26, 27] therefore possibly allowing *in* vivo detection of tumors.

Despite extensive research into the interaction between cells and TiO$_2$ nanoparticles, the lack of variety in techniques to allow *in vitro* and *in vivo* TiO$_2$ detection has hindered statistical analysis of large scale cell-TiO$_2$ nanoparticle interaction studies. Most studies to date rely primarily on transmission electron microscopy (TEM) to determine nanoparticle internalization, and some verify this with Energy Filtering TEM (EFTEM).[13,14,28,29] Despite the high spatial resolution of these techniques, they only permit analysis of relatively small cell numbers, and require sectioning of the biological samples. TiO$_2$ nanoparticles have recently have been conjugated to 5-malmadeine fluorescein dyes,[8] but fluorescein can be quenched upon binding of the TiO$_2$ nanoparticle with enediol ligands (e.g. dopamine).[4] It is also possible to detect a change in side scatter characteristic of cell populations using flow cytometry as a function of TiO$_2$ nanoparticle uptake.[30] Since, however, side scatter is only an indicator of cell granularity[31] it cannot directly detect the nanoparticles themselves, and thus requires treatment with relatively high numbers of nanoparticles. Therefore additional methods for detecting intracellular TiO$_2$ are greatly needed.

Recently, our group has used X-Ray Fluorescence Microscopy (XFM) to detect and map nanoparticles directly in whole cells based on their titanium content.[9,10] XFM is a powerful and sensitive technique (which detects as few as several thousand atoms[32]) using bright X-rays to excite element specific Kα X-ray fluorescence and create a quantitative and qualitative elemental map of biological samples at submicron resolutions.[32-35]

Using XFM and TEM, our group has shown that the TiO_2-DNA nanoconjugates can be specifically retained in subcellular compartments where complementary nuclear or mitochondrial DNA is present.[9,10] It is crucial for further investigations of TiO_2 that large populations of cells be examined rapidly and consistently. In order to achieve this goal we devised methods to modify the TiO_2 nanoparticle with optical fluorescent dyes which are normally invisible by optical microscopy except at very high quantities. We have accomplished this by using fluorescently labeled DNA oligonucleotides, and by labeling the nanoparticles directly with Alizarin Red S (ARS). The ARS surface modification can be performed either before or after nanoparticles have been taken up by cells. Subsequently, this permitted the use of high throughput techniques such as flow cytometry to quantify cellular uptake of nanoparticles. It also allowed direct investigation into the cytotoxicity of nanoparticles in conjunction with nanoparticle uptake. Fluorescent modification of nanoparticles combined with XFM allowed determination of the relative intracellular TiO_2-DNA nanoconjugate stability.

2. Results and Discussion

One of the limiting factors in TiO_2 nanoparticles studies is the lack of diversity in available intracellular detection techniques. Taking advantage of the surface chemistry of TiO_2 nanoparticles, the nanoparticle/nanoconjugates were fluorescently labeled by two separate approaches. At 20 nm or below, the metal oxide nanoparticle's surface geometry changes from a pentacoordinated to a hexacoordinated position.[19] These undercoordinated "surface defects" have a high affinity for ortho-substituted enediol ligands (e.g. dopamine, alizarin, ascorbic acid) that restore the surface titanium atom's coordination back to its relaxed, octahedral form upon binding.[19,36] DNA oligonucleotides that had their 5' dT terminal ends carboxyl modified, were bound to dopamine as described earlier.[9,10,20] Their 3' terminal ends were labeled with either fluorescent tetramethylrhodamine (TAMRA) or Cy5. The 5' dopamine modified end was then used to covalently link the DNA oligonucleotide directly to the surface of the nanoparticle creating a stable TiO_2-dopamine-DNA nanoconjugate with a fluorescently labeled nucleic acid component (Figure 1).

In an attempt to establish a simple, inexpensive, and covalent process to fluorescently label the nanoparticle directly for intracellular detection, we modified the surface of the metal-oxide nanoparticles with Alizarin Red S (ARS). We suspected that binding of ARS to nanoparticles would render them highly fluorescent since locally high concentrations of ARS molecules increase their local concentration and light absorbance. ARS (a derivative of alizarin) is an ortho-substituted enediol ligand that has never been previously reported to be used as an intracellular label for TiO_2 nanoparticles. ARS has been used in optical microscopy for fluorescent labeling of calcium deposits.[37,38] Since the same hydroxyl groups of ARS are significant in the binding to both calcium and TiO_2,[38] the nanoparticle bound ARS should be precluded from binding calcium. It has been reported that ARS is able to form complexes with proteins at low pH (3.6), although this was almost completely inhibited as pH values approached physiological conditions.[39] For direct surface binding to the nanoparticle, ARS was added to 5 nm TiO_2 nanoparticles. The nanoparticles' UV-VIS absorbance spectra were analyzed since surface modification of the nanoparticle will cause a change in absorbance. Results from Figure 2 show that TiO_2 nanoparticles show absorption wavelengths smaller than 350 nm. Conjugation of 44% of the total surface titanium atoms with ARS (TiO_2-ARS) caused

a red shift and creation of a unique absorption maximum at 510 nm. This fluorescence could be excited at relatively long wavelengths (absorption peak at 510 nm is very broad) which have higher tissue/cell penetrance than the UV wavelengths. The UV-VIS absorbance spectra of the TiO_2-ARS complex was very similar to those published of TiO_2-Alizarin.[18,40] This is not surprising since the two polycyclic aromatic molecules differ only in the addition of a sulfonate group on ARS (1,2 dihydroxyanthraquinone vs. 1,2 dihydroxyanthraquinone-3-sulfonate). ARS alone at the same concentration had an absorbance peak at 420 nm.

To determine if the ARS modified nanoparticles in cells are detectable by fluorescent confocal microscopy, prostate cancer PC-3M and breast cancer MCF-7 cells were serum-starved and treated with ARS coated TiO_2 nanoparticles (TiO_2-ARS). As controls, cells were left untreated, treated with ARS alone, or treated with uncoated TiO_2. Absolute ARS and nanoparticle concentrations were the same in each case. The treated cells were then imaged using two separate excitation lasers: 488 nm and 543 nm. A previous study claimed to have detected TiO_2 nanoparticles directly using an excitation laser of 488 nm with emission filters between 505-550 nm.[30] Figure 3A, third row, shows the results when similar experimental and microscopy parameters were used. Cells were treated with the nanoparticles which lead to a significant accumulation of nanoparticles on the cell surface as well as internalized nanoparticles. It is noteworthy that further experiments used an acidic glycine wash (200 mM, pH 4.0) in order to decrease surface bound nanoparticles. Extensive washing in low pH glycine was demonstrated to reduce oligonucleotide binding to the cell surface.[41] We found that it also significantly reduced the extent of nanoparticle binding to the cell membrane (data not shown). Unlabeled TiO_2 nanoparticles did not exhibit a detectable fluorescent signal using a 488 nm excitation laser and a 505-530 nm bandpass filter for signal detection. The difference compared to the previous study[30] may perhaps be caused by different properties/sizes of nanoparticles (23 nm vs. 5 nm), different degree of nanoparticle accumulation within cells, or different degree of background fluorescence. Treatment of cells with TiO_2-ARS (fourth row) did, however, result in a strong fluorescent signal in the range of 560-615 nm when excited with a 543 nm laser. Thus ARS modified nanoparticles are fluorescent emitting at 560-615 nm wavelengths where little background fluorescence from can be expected. Importantly, cells treated with ARS alone did not produce a detectable fluorescent signal with either excitation laser. Non-specific retention of ARS did not occur within the cells under the conditions tested, and ARS was not able to form significant fluorescent intracellular complexes without conjugation to the TiO_2 nanoparticle.

In order to determine if post-treatment fluorescent labeling of nanoparticles already internalized into cells with ARS was possible, PC-3M cells were treated with unlabeled nanoparticles, fixed, and subsequently stained with an ARS solution in phosphate buffered saline solution (PBS). Results in Figure 3B show a detectable intracellular ARS fluorescence within the cytoplasm. Fixed cells that were not previously treated with TiO_2 did not exhibit a detectable fluorescent signal upon treatment with the ARS solution (Figure 3A). This suggests that internalization of nanoparticles was not due to ARS coating, and that ARS was able to bind intracellular TiO_2 particles in fixed cells.

Our group has previously conjugated glycidyl isopropyl ether (GIE) to the surface of TiO_2 nanoparticles (TiO_2-GIE) in order to reduce bio-reactivity of the nanoparticle within cells.[9, 10] The use of uncoated TiO_2 nanoparticles is also of significance since their excitation produces an abundance of reactive oxygen species which can be used for cell killing without gene specific targeting.[6,8] Therefore, we determined the viability of cells that have taken up GIE coated or uncoated TiO_2 nanoparticles. Viability assays require investigation of thousands of cells and could never be done in conjunction with TEM or XFM. Labeling the nanoparticles, however, allowed us to screen the treated cells simultaneously for nanoparticle uptake (by ARS fluorescence) and for viability (by use of fluorescent cell-impermeable dye). PC-3M cells were

treated with GIE coated and uncoated TiO_2 nanoparticles labeled with ARS. As a control, 20 mM hydrogen peroxide (H_2O_2) was used as an inducer of cell death.[42] Flow cytometry was then used to quantify both the extent of nanoparticle uptake within the cell population, and the cells' ability to exclude cell-impermeable DAPI as an indicator of cell viability. Results show that when treated with ARS alone, virtually the entire population of cells was viable and capable of dye exclusion (Figure 4A). Both of the TiO_2 nanoparticles treated cells (TiO_2-GIE-ARS and TiO_2-ARS) showed no significant decrease in viability, with the number of dead cells averaging 5% and 2%, respectively (n=3). H_2O_2 treated cells, on the other hand, showed an approximately 54% reduction in viability. This suggested that neither TiO_2-ARS nor TiO_2-GIE-ARS nanoparticles had a significant effect on cell viability at the concentration used in the experiments described herein. These results were confirmed in MCF-7 cells (data not shown).

While simultaneously detecting cell viability, samples were also analyzed for ARS fluorescence as an indicator of nanoparticle uptake. Internalization of nanoparticles was shown by the number of cells excited to fluoresce using similar parameters to those performed during microscopy. Figure 4B is a representative plot of several experiments performed (n=3), showing that cells treated with ARS alone exhibited very low auto-fluorescence (excitation with 543 nm laser, emission in 560-615 nm range). Cells treated with TiO_2-GIE-ARS showed an average nanoparticle uptake of 36% within the cell population, while TiO_2 nanoparticles lacking GIE had a similar nanoparticle internalization of 32%. This suggested that GIE did not significantly aid in the internalization of the nanoparticle, nor did it affect viability of cells. Importantly, ARS could be used by both confocal microscopy and flow cytometry to detect intracellular TiO_2 nanoparticles.

To determine the subcellular localization of the separate components of the TiO_2-DNA nanoconjugates, cells were treated simultaneously with both TiO_2-ARS nanoparticles and free Cy5 labeled unbound DNA oligonucleotides. After treatment and washes, the cells were imaged by confocal microscopy. Results in Figure 5 show that there was a strong accumulation of the ARS labeled nanoparticles in endosomal vesicles within the cytoplasm. Although it is possible that the endocytic mechanisms of TiO_2 nanoparticles change due to ARS labeling, the subcellular distribution was similar to that seen when the Alizarin Red S was used for post-treatment staining (Figure 3B); in addition work by others with unlabeled nanoparticles using transmission electron microscopy showed similar nanoparticle distribution.[14] This would suggest that the uptake mechanism was not altered due to Alizarin Red S surface labeling. The free oligonucleotides, on the other hand, showed a strong localization within the nuclei, and more strikingly within the nucleoli. This was similar to the results previously obtained with free oligonucleotides[43-45] and by our group with complete nanoconjugates.[9,10] These results demonstrated that the separate components of the nanoconjugates (the nanoparticle and DNA oligonucleotide) accumulated in separate subcellular organelles and did not co-localize within the same cell if not covalently bound together. This suggests that the separate components enter the cell via unique internalization mechanisms, or are distinctly trafficked within the cell. Although these mechanisms have been extensively studied for oligonucleotides in various cell lines,[46-49] this is not the case for TiO_2 nanoparticles. Further experiments aimed at determining these mechanisms are vitally needed since the modes of trafficking and internalization have a direct impact on subcellular localization and potential cytotoxicity.

Since the functionality and targeting of the nanoconjugates are greatly dependent on their integrity, we combined confocal microscopy with X-Ray Fluorescent Microscopy (XFM) to track both components independently within the same cell. Confocal microscopy was used to detect the DNA oligonucleotide component, while XFM was used to directly detect titanium (and thereby the nanoparticles). XFM was performed at the 2-ID-D beamline at the Advanced Photon Source at Argonne National Laboratories. XFM mapped the location and concentration

of elements ranging from phosphorus to zinc on the periodic table (including titanium) using raster scanning with step sizes of 0.3 μm.

Figure 6A shows the results from confocal microscopy compared to that obtained from XFM. Confocal microscopy revealed several small accumulations of the TAMRA labeled DNA oligonucleotides within the cytoplasm and a stronger signal aligned with the nucleus. XFM analysis revealed a distribution of titanium that was very similar to that of TAMRA. The phosphorus map also revealed a strong co-localization with titanium and TAMRA. This is probably an artifact due to the fixing, staining, and mounting techniques involved in sample preparation. Titanium concentration, however, was determined only by the presence of nanoparticles. Figure 6B shows quantification of the number of nanoparticles located within the specified regions of interest (ROI). ROI 1 corresponds to a detectable XFM titanium signal (3.1×10^4 nanoparticles) although the TAMRA signal of this nanoparticle accumulation was only very weakly visible. Each nanoparticle was modified by approximately 2 TAMRA labeled oligonucleotides so that the optically fluorescent signal corresponds to 6.2×10^4 TAMRA molecules. The strongest titanium signal came from ROI 3 and showed the presence of approximately 1.3×10^6 nanoparticles. Confocal microscopy also showed a clearly detectable TAMRA signal within the same relative subcellular area. There are several titanium distributions obtained by XFM that were not imaged by confocal microscopy. This is likely due to the fact that the hard X-rays used in XFM are able to penetrate the entire cell, while confocal microscopy imaged optical cell slices of 0.13 μm thickness. To verify this, multiple planes of cells treated with ARS labeled TiO_2-DNA nanoconjugates were visualized by confocal microscopy and subsequently imaged by XFM. Results showed that accumulations of the ARS labeled TiO_2-DNA nanoconjugates were not visible in one plane of microscopy, but were visible in different planes. At the same time, however, both of the aggregates were shown to overlap with titanium (Figure 7). As few as 7.9×10^4 nanoparticles were detectable by fluorescence microscopy when 44% of the total surface of the TiO_2 nanoparticle was coated with ARS (Figure 7, ROI 1). The overall similarity in the distributions of both TAMRA labeled DNA oligonucleotide and titanium nanoparticle strongly suggest that the integrity of the TiO_2-DNA nanoconjugates remains intact at the time point examined (12 hours).

3. Conclusions

These results demonstrate that it is possible to fluorescently label TiO_2 nanoparticles in a simple and specific manner using ARS. Most excitingly, this labeling can be used both prior to nanoparticle treatment of cells, and after nanoparticle internalization and fixation. To our knowledge, this is the first report of fluorescently labeled TiO_2 uptake quantification in a large cell population (with assays using at least 10^4 cells per sample). This approach will allow for extensive study into the exact mechanisms by which these nanoparticles enter living cells, and the effects of potential future surface modifications. A similarly simple Alizarin Red S labeling should also be feasible for other semiconducting metal-oxide nanoparticles (e.g. FeO_3, ZrO_2) [18] Application of Alizarin Red S as a fluorescent label to other types of nanoparticles (e.g. carbon based nanoparticles) would require more extensive conjugation chemistry. Localization of nanoparticles in tissues of treated animals should become optically visible using the ARS staining. In addition, we also showed that transfected TiO_2-DNA nanoconjugates remain stable in malignant cells for at least 12 hours. The high sensitivity of XFM and the full sample penetration of the X-rays allowed detection of nanoparticles not visualized by microscopy. The combination of both techniques, however, did allow for validation of the ARS modification of the nanoparticles within cells, and it determined that as few as 7.9×10^4 ARS modified nanoparticles or as few as 3.1×10^4 nanoparticles modified by 6.2×10^4 TAMRA labeled oligonucleotides were detectable by fluorescent microscopy.

4. Experimental

Nanoconjugate Preparation

All reagents were purchased from Sigma Aldrich unless otherwise specified. TiO_2 nanoparticles with mean diameter of around 5-6 nm were synthesized at Northwestern University's Nanofabrication Core of NU-Center for Cancer Nanotechnology Excellence, applying low-temperature alkaline hydrolysis route, dialyzed, and stored in Na_2HPO_4 buffer (10 mM) at 4°C. Surface coating with glycidyl isopropyl ether was performed as described previously.[9] Conjugation of single stranded 5' carboxyl deoxythymidine modified DNA oligonucleotides (ttccttggatgtggt) (The Midland Certified Reagent Co.) to dopamine, and subsequent conjugation to TiO_2 nanoparticles was performed as described previously.[9,10, 20] The oligonucleotides were also purchased with either tetramethylrhodamine (TAMRA) or Cy5 3' end modification.

Alizarin Red S Surface Coating and UV-VIS Absorbance Spectrum Analysis

For determination of covalent surface modification, TiO_2 nanoparticles (5 μM) were dialyzed and stored in Na_2HPO_4 buffer (10 mM) and mixed with Alizarin Red S (0.9 mM). The samples were then analyzed by the Nanodrop ND-1000 Spectrophotometer (NanoDrop Technologies Inc.,) for absorbances ranging from 200-750 nm.

Cell Culture and Treatment with Nanoparticles/Nanoconjugates

All cell culture reagents were purchased from Mediatech Inc. unless otherwise specified. PC-3M metastatic prostate cancer cells were a gift from Dr. Raymond Bergan, Northwestern University. MCF-7/WS8 cells were obtained from American Type Culture Collection (ATCC). Both cell lines were maintained at 37°C with 5% CO_2 in RPMI 1640 media supplemented with fetal bovine serum (10%), L-glutamine (2 mM), HEPES (10 mM), penicillin (100 I.U./ml), streptomycin (100 μg/ml). MCF-7 cells were further supplemented with non-essential amino acids (1X), amphoterecin B (0.25 μg/ml), and insulin (0.1 mg/ml) (Sigma-Aldrich). PC-3M cells were further supplemented with G418 sulfate (0.15 mg/ml). For treatment, cells were washed with phosphate buffered saline solution (PBS) and placed in serum free RPMI 1640 for 1-2 hours. Then cells were treated with TiO_2 nanoparticles (333 nM) coated with or without ARS (60 μM), and/or ODN (160 μM) for one hour. After treatment, cells were washed with PBS, and then in glycine (200 mM, pH 4) (Sigma Aldrich). After more washing in PBS, the cells were further prepared as described below, depending on the technique performed. Transfection of cells was carried out using Superfect (Qiagen) according to manufacturer's suggestions.

Flow Cytometry and Cell Sorting

Cells to be analyzed by flow cytometry were grown until approximately 60% confluence. After treatment and washing, cells were trypsinized, collected in FBS supplemented medium, and brought to a single cell suspension. To determine cell viability, cell samples were treated with DAPI (5 μg/ml) (Molecular Probes, Invitrogen) prior to analysis. Samples were then taken to the Northwestern University Flow Cytometry Core Facility of the Robert H. Lurie Cancer Center to be analyzed or sorted on the DakoCytomation MoFlo Flow Cytometer (Dako). Excitation lasers of 350 nm and 543 nm were used to excite DAPI and TAMRA/ARS, respectively. Debris was excluded based on the forward and side scatter characteristics of the cell populations. Analysis of flow cytometry data was performed using the FCS Express V3 program (De Novo Software).

Confocal Microscopy

For visualization by confocal microscopy, cells were cultured on glass coverslips. Cells at approximately 60% confluence were treated and washed as described above. The cells were then fixed in paraformaldehyde (4%), and stained with Hoechst 33343 (Molecular Probes, Invitrogen). After washing the cells were placed in anti-fade mounting medium (Molecular Probes, Invitrogen) and visualized using the LSM 510 UV Meta Microscope (Carl Zeiss, Inc.) at the Northwestern University Cell Imaging Facilities using 405 nm, 488 nm, and 543 nm lasers with bandpass filters of 420-480 nm, 505-530 nm, 560-615 nm, respectively.

X-Ray Fluorescence Microscopy (XFM)

Cells transfected with TiO_2-DNA (TAMRA) nanoconjugates were sorted for the presence of TAMRA, seeded on formvar coated gold EM grids (Electron Microscopy Sciences) and allowed to adhere. The samples were then fixed in cold methanol (-20°C), and stained with Hoechst 33342 dye. The samples were placed in anti-fade mounting medium between a glass coverslip and slide, and imaged by confocal microscopy. Next, the cells were washed in glycine and PBS, dehydrated in ethanol (100%), and allowed to air dry. Before XFM analysis, the presence of the cells was verified, and coordinates for their locations were obtained by the Leica DMXRE light microscope and a motorized x/y stage (Ludl Electronic Products). XFM was performed at the 2-ID-D beamline at the Advanced Photon Source at Argonne National Laboratories where an undulator source was used to create hard X-Rays with energies of 10 keV and focused using Fresnel zone plate optics. Emitted X-Ray fluorescence was detected using an energy dispersive germanium detector (LEGe Detector, Canberra). Elemental quantification and localizations were calculated using the MAPS program.[50]

Supplementary Material

Refer to Web version on PubMed Central for supplementary material.

Acknowledgments

References

1. Blake DM, Maness PC, Huang Z, Wolfrum EJ, Huang J, Jacoby WA. Separation and Purification Methods 1999;28(1):1–50.

2. Gogniat G, Thyssen M, Denis M, Pulgarin C, Dukan S. FEMS Microbiol Lett 2006;258(1):18–24. [PubMed: 16630249]

3. Tsuang YH, Sun JS, Huang YC, Lu CH, Chang WH, Wang CC. Artif Organs 2008;32(2):167–174. [PubMed: 18269355]

4. Wu HP, Cheng TL, Tseng WL. Langmuir 2007;23(14):7880–7885. [PubMed: 17564470]

5. Ashcroft JM, Gu W, Zhang T, Hughes SM, Hartman KB, Hofmann C, Kanaras AG, Kilcoyne DA, Le Gros M, Yin Y, Alivisatos AP, Larabell CA. Chem Commun (Camb) 2008;21:2471–2473. [PubMed: 18491018]

6. Zhang AP, Sun YP. World J Gastroenterol 2004;10(21):3191–3193. [PubMed: 15457572]

7. Cai R, Kubota Y, Shuin T, Sakai H, Hashimoto K, Fujishima A. Cancer Res 1992;52(8):2346–2348. [PubMed: 1559237]

8. Seo JW, Chung H, Kim MY, Lee J, Choi IH, Cheon J. Small 2007;3(5):850–853. [PubMed: 17385208]

9. Paunesku T, Rajh T, Wiederrecht G, Maser J, Vogt S, Stojicevic N, Protic M, Lai B, Oryhon J, Thurnauer M, Woloschak G. Nat Mater 2003;2(5):343–346. [PubMed: 12692534]

10. Paunesku T, Vogt S, Lai B, Maser J, Stojicevic N, Thurn KT, Osipo C, Liu H, Legnini D, Wang Z, Lee C, Woloschak GE. Nano Lett 2007;7(3):596–601. [PubMed: 17274661]

11. Liu J, Saponijc Z, Dimitrijevic NM, Luo S, Preuss D, Rajh T. Proc of SPIE 2006;6096:60960F60961–60960F60910.

12. Huang, N-p; Min-hua, X.; Yuan, C-w; Rui-rong, Y. Journal of Photochemistry and Photobiology A: Chemistry 1997;108(23):229.

13. Long TC, Tajuba J, Sama P, Saleh N, Swartz C, Parker J, Hester S, Lowry GV, Veronesi B. Environ Health Perspect 2007;115(11):1631–1637. [PubMed: 18007996]

14. Singh S, Shi T, Duffin R, Albrecht C, van Berlo D, Hohr D, Fubini B, Martra G, Fenoglio I, Borm PJ, Schins RP. Toxicol Appl Pharmacol 2007;222(2):141–151. [PubMed: 17599375]

15. Jeng HA, Swanson J. J Environ Sci Health A Tox Hazard Subst Environ Eng 2006;41(12):2699–2711. [PubMed: 17114101]

16. Peters K, Unger RE, Kirkpatrick CJ, Gatti AM, Monari E. J Mater Sci Mater Med 2004;15(4):321–325. [PubMed: 15332593]

17. Fabian E, Landsiedel R, Ma-Hock L, Wiench K, Wohlleben W, van Ravenzwaay B. Arch Toxicol 2008;82(3):151–157. [PubMed: 18000654]

18. Rajh T, Chen LX, Lukas K, Liu T, Thurnauer MC, Tiede DM. J Phys Chem B 2002;106(41):10543–10552.

19. Rajh T, Nedeljkovic JM, Chen LX, Poluektov O, Thurnauer MC. J Phys Chem B 1999;103(18):3515–3519.

20. Rajh T, Saponjic Z, Liu J, Dimitrijevic NM, Scherer NF, Vega-Arroyo M, Zapol P, Curtiss LA, Thurnauer MC. Nano Lett 2004;4(6):1017–1023.

21. Liu J, de la Garza L, Zhang L, Dimitrijevic NM, Zuo X, Tiede DM, Rajh T. Chem Phys 2007;339 (13):154.

22. Weinstein IB, Joe AK. Nat Clin Pract Oncol 2006;3(8):448–457. [PubMed: 16894390]

23. Wang YH, Liu S, Zhang G, Zhou CQ, Zhu HX, Zhou XB, Quan LP, Bai JF, Xu NZ. Breast Cancer Res 2005;7(2):R220–228. [PubMed: 15743499]

24. Felsher DW. Nat Rev Cancer 2003;3(5):375–380. [PubMed: 12724735]

25. Chin L, Tam A, Pomerantz J, Wong M, Holash J, Bardeesy N, Shen Q, O'Hagan R, Pantginis J, Zhou H, Horner JW 2nd, Cordon-Cardo C, Yancopoulos GD, DePinho RA. Nature 1999;400(6743):468–472. [PubMed: 10440378]

26. Endres PJ, Paunesku T, Vogt S, Meade TJ, Woloschak GE. J Am Chem Soc 2007;129(51):15760–15761. [PubMed: 18047347]

27. Paunesku T, Ke T, Dharmakumar R, Mascheri N, Wu A, Lai B, Vogt S, Maser J, Thurn K, Szolc-Kowalska B, Larson A, Bergan RC, Omary R, Li D, Lu Z-R, Woloschak GE. Nanomedicine: Nanotechnology, Biology and Medicine. 2008In Press, Corrected Proof

28. Rothen-Rutishauser BM, Schurch S, Haenni B, Kapp N, Gehr P. Environ Sci Technol 2006;40(14): 4353–4359. [PubMed: 16903270]

29. Geiser M, Casaulta M, Kupferschmid B, Schulz H, Semmler-Behnke M, Kreyling W. Am J Respir Cell Mol Biol 2008;38(3):371–376. [PubMed: 17947511]

30. Suzuki H, Toyooka T, Ibuki Y. Environ Sci Technol 2007;41(8):3018–3024. [PubMed: 17533873]

31. Haynes JL. Cytometry Suppl 1988;3:7–17. [PubMed: 3076370]

32. Fahrni CJ. Curr Opin Chem Biol 2007;11(2):121–127. [PubMed: 17353139]

33. Paunesku T, Vogt S, Maser J, Lai B, Woloschak G. J Cell Biochem 2006;99(6):1489–1502. [PubMed: 17006954]

34. McRae R, Lai B, Vogt S, Fahrni CJ. J Struct Biol 2006;155(1):22–29. [PubMed: 16473527]

35. Yang L, McRae R, Henary MM, Patel R, Lai B, Vogt S, Fahrni CJ. Proc Natl Acad Sci U S A 2005;102 (32):11179–11184. [PubMed: 16061820]

36. Rajh T, Poluektov O, Dubinski AA, Wiederrecht G, Thurnauer MC, Trifunac AD. Chem Phys Lett 2001;344(12):31.

37. Papalexiou V, Novaes AB Jr, Grisi MF, Souza SS, Taba M Jr, Kajiwara JK. Clin Oral Implants Res 2004;15(1):44–53. [PubMed: 14731176]

38. Puchtler H, Meloan SN, Terry MS. J Histochem Cytochem 1969;17(2):110–124. [PubMed: 4179464]

39. Zhong H, Li N, Zhao F, Li Ka. Talanta 2004;62(1):37. [PubMed: 18969260]

40. Huber R, Sporlein S, Moser JE, Gratzel M, Wachtveitl J. J Phys Chem B 2000;104(38):8995–9003.

41. Morassutti C, Scaggiante B, Dapas B, Xodo L, Tell G, Quadrifoglio F. Biochimie 1999;81(12):1115. [PubMed: 10607406]

42. Whittemore ER, Loo DT, Watt JA, Cotmans CW. Neuroscience 1995;67(4):921. [PubMed: 7675214]

43. Laktionov PP, Dazard JE, Vives E, Rykova EY, Piette J, Vlassov VV, Lebleu B. Nucleic Acids Res 1999;27(11):2315–2324. [PubMed: 10325420]

44. Nestle FO, Mitra RS, Bennett CF, Chan H, Nickoloff BJ. J Invest Dermatol 1994;103(4):569–575. [PubMed: 7930684]

45. Noonberg SB, Garovoy MR, Hunt CA. J Invest Dermatol 1993;101(5):727–731. [PubMed: 8228335]

46. de Diesbach P, N'Kuli F, Berens C, Sonveaux E, Monsigny M, Roche AC, Courtoy PJ. Nucleic Acids Res 2002;30(7):1512–1521. [PubMed: 11917011]

47. Garcia-Chaumont C, Seksek O, Grzybowska J, Borowski E, Bolard J. Pharmacol Ther 2000;87(23):255–277. [PubMed: 11008003]

48. Lysik MA, Wu-Pong S. J Pharm Sci 2003;92(8):1559–1573. [PubMed: 12884243]

49. Khalil IA, Kogure K, Akita H, Harashima H. Pharmacol Rev 2006;58(1):32–45. [PubMed: 16507881]

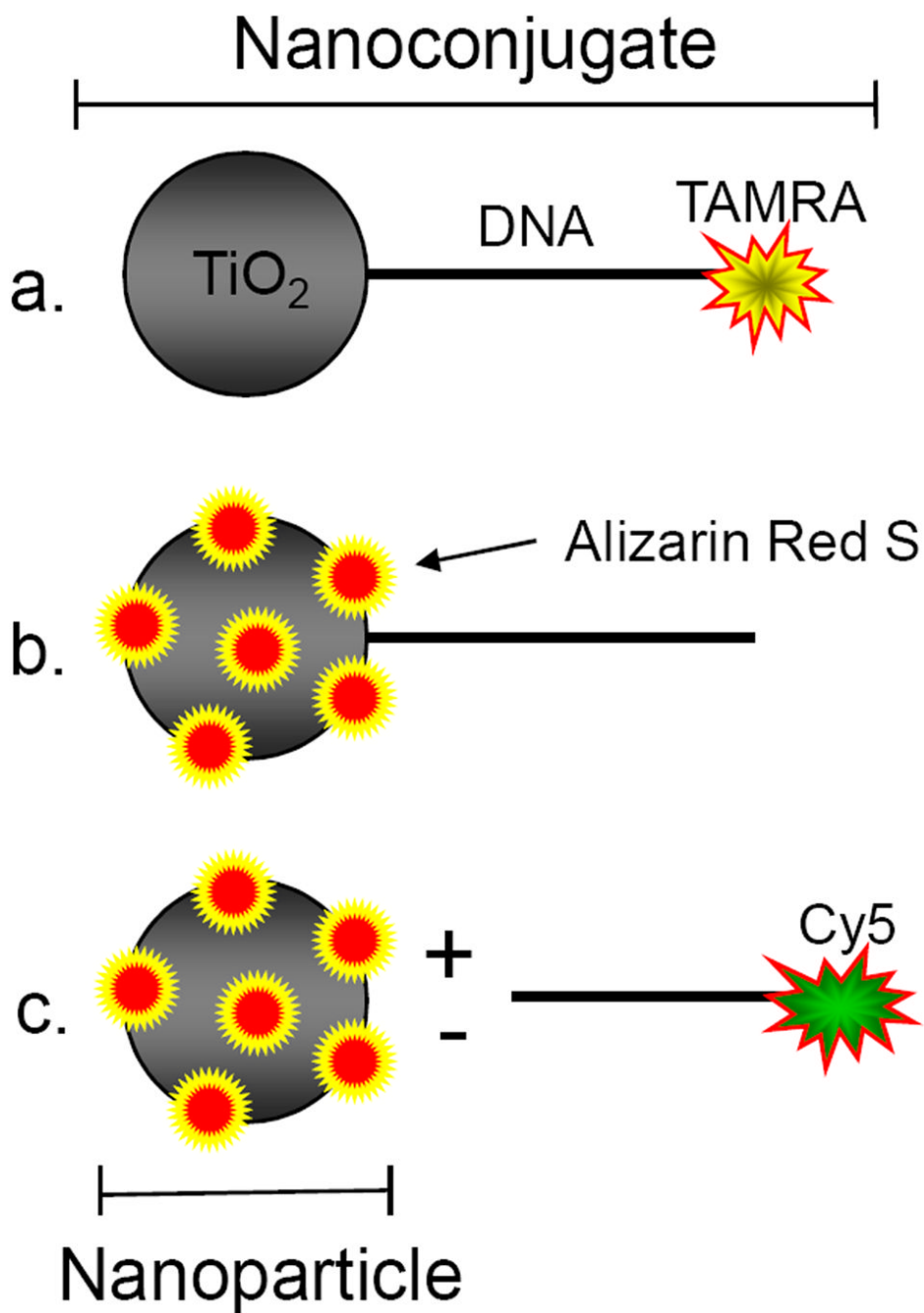50. Vogt S. J Phys IV 2003;104:635–638.

Figure 1.
Schematic Representation of Fluorescent Labeling of TiO$_2$-DNA Nanoconjugates. *a*. DNA ODNs are labeled at the 3' end with TAMRA, while the 5' carboxyl dT terminal ODN end is modified with dopamine (not depicted) which can subsequently bind the oxygen-depleted "surface defects" of TiO$_2$ nanoparticles < 20 nm[cite]. This creates a TiO$_2$-dopamine-ODN (TAMRA) nanoconjugate. *b*. Direct covalent conjugation of Alizarin Red S (ARS) to the undercoordinated "surface defects" of TiO2 nanoparticles creating an ARS labeled TiO$_2$-ODN nanocomposite. *c*. Direct ARS labeling of nanoparticle unbound to ODN with the addition of free Cy5 labeled ODN to track both components independently.
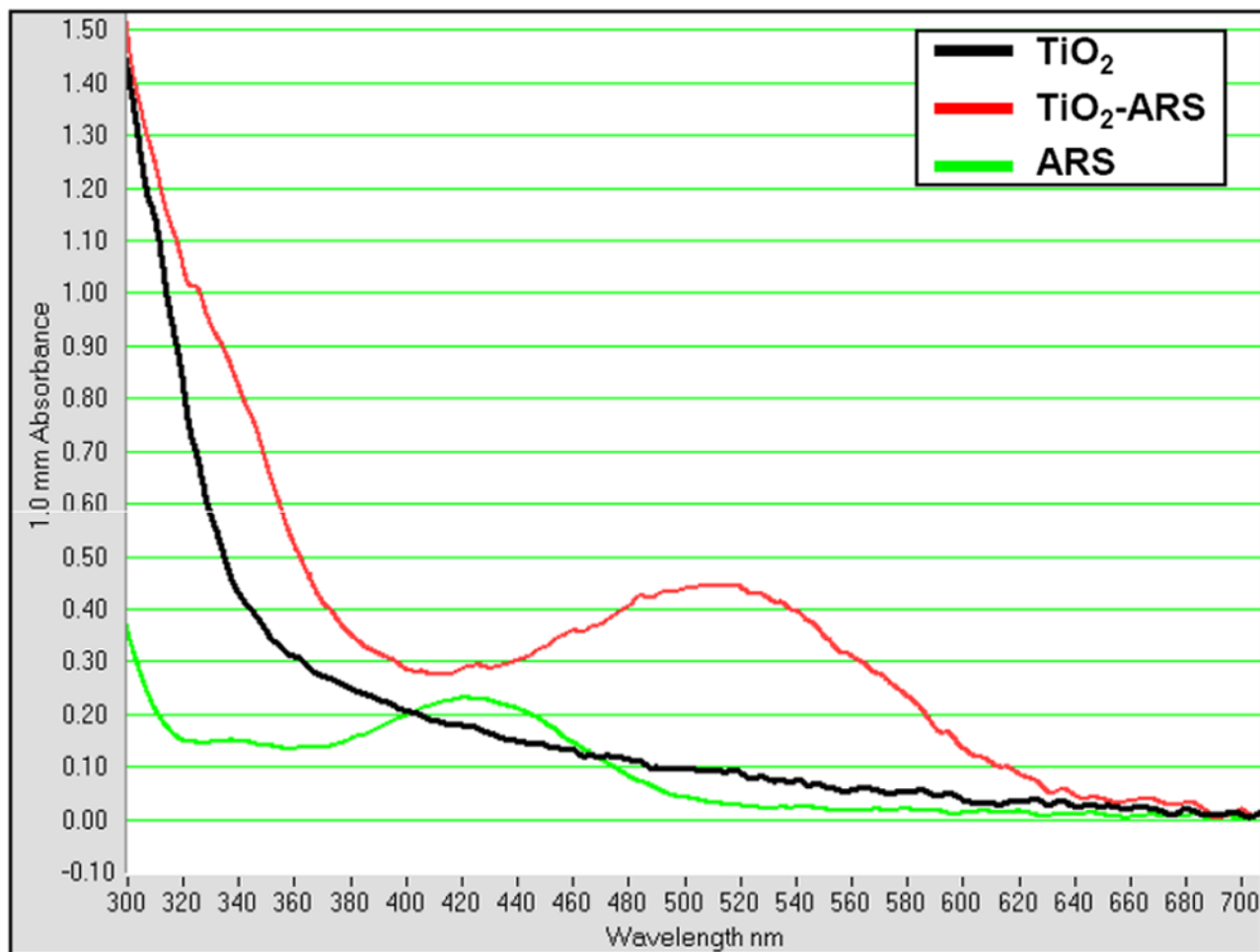
Figure 2.
UV-VIS Absorbance Spectrum of ARS Coated TiO$_2$ Nanoparticles. TiO$_2$ nanoparticles at 5 mM alone cause an onset of absorption near 350 nm. The addition of ARS (0.9 mM) to TiO2 nanoparticles (TiO$_2$-ARS) to coat approximately 5% of the total available surface titanium atoms, however, results in a distinct absorbance maximum at approximately 510 nm indicating the covalent surface modification of the nanoparticles. ARS alone at the same concentration (0.9 mM) has an absorbance peak at 420 nm.
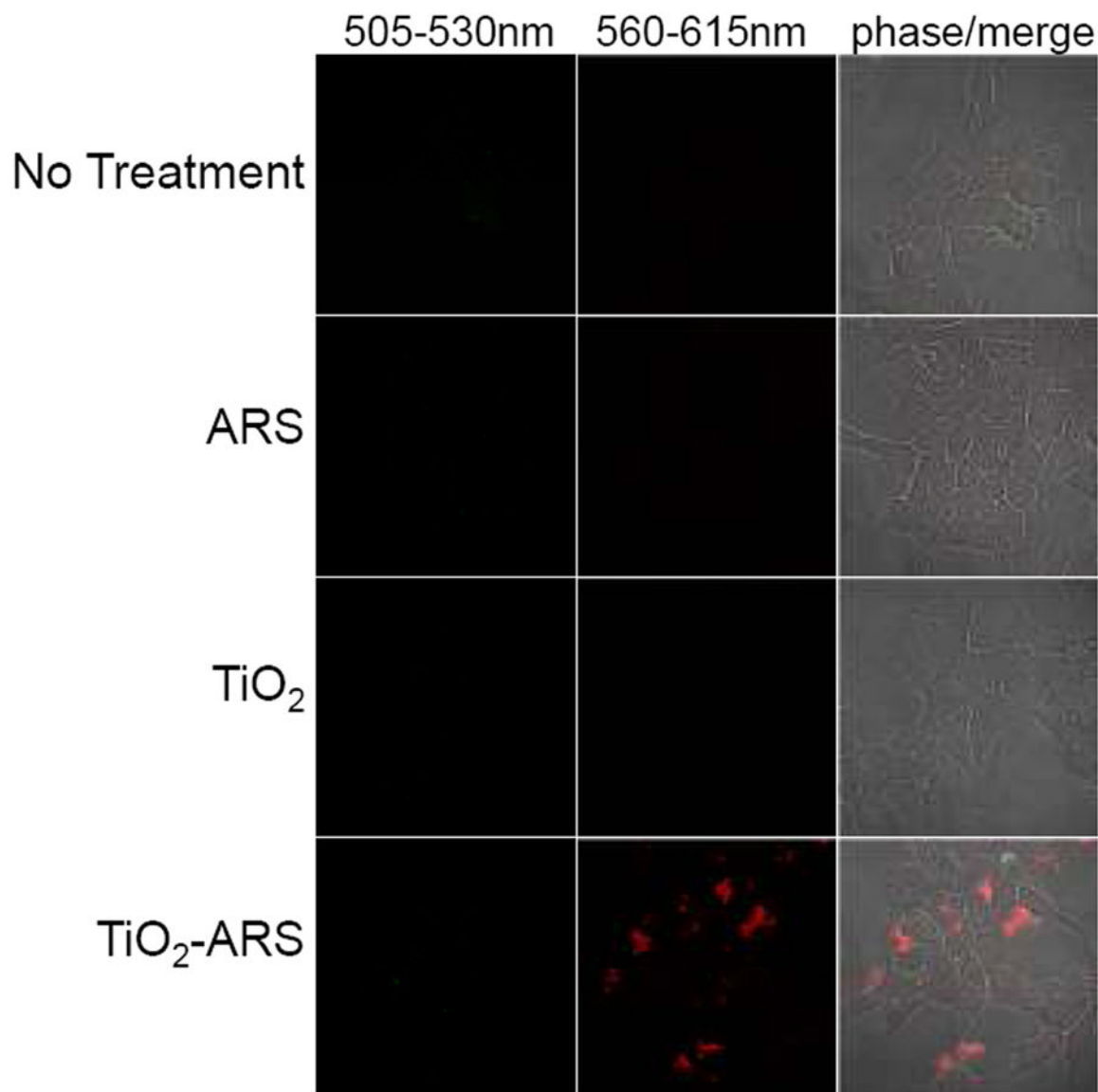
Figure 3.
Intracellular detection of ARS modified TiO_2 Nanoparticles. Prostate Carcinoma PC3-M cells were placed in serum-free medium for 1 hour and were either untreated (top), treated with 60 μM ARS alone, treated with 333 μM of undmodified TiO_2 nanoparticles, or nanoparticles coated with ARS (5% nanopartile surface coating) for 1 hour. Results show that there was no detectable fluorescent signal from TiO_2 directly using bandpass filters of 505-530 nm or 560-615 nm (excitation= 488 nm and 543 nm). A strong fluorescent signal was only detected for nanoparticles modified with ARS using a 560-615 nm bandpass filter (excitation= 543 nm) while unmodified nanoparticles, and ARS alone showed no signal.
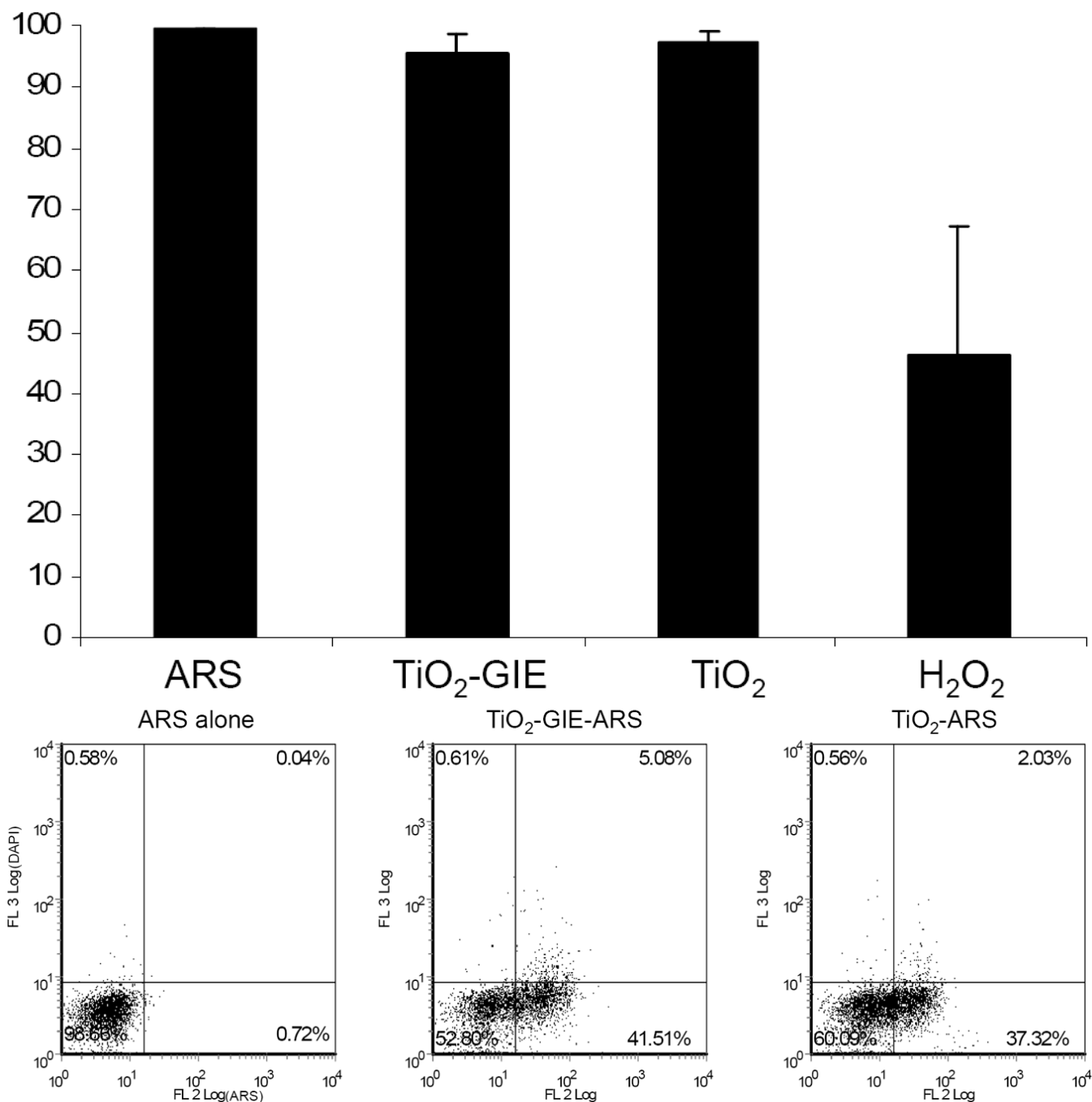
Figure 4.
A. Effect of TiO$_2$ Nanoparticles on Cell Viability. PC3-M cells were treated with 333 μM of ARS labeled Glycidyl Isopropyl Ether (GIE) coated TiO$_2$, uncoated TiO$_2$ nanoparticles, or 200 mM hydrogen peroxide (H$_2$O$_2$) as a cell death control for 24 hours. Then cells were washed, collected, and analyzed by flow cytometry for their ability to exclude fluorescent DAPI as a marker for cell viability. Results show that neither TiO$_2$ treated cell population showed a decrease in ability to exclude DAPI, while hydrogen peroxide treated cells showed an approximately 54% reduction in cell viability.

B. Quantification of TiO$_2$-ARS Nanoparticle Uptake. Uptake of TiO$_2$-ARS nanoparticles by PC3-M cells was also analyzed in the same cells from Figure 4A based on their extent of ARS fluorescence. Above is a representative plot of the results obtained from three independent experiments. Cells treated with ARS alone do not exhibit significant fluorescence in the FL2 channel (excitation at 543 nm), while cells treated with ARS modified nanoparticles show a significant increase in the number of cells which internalize the fluorescently labeled metal-oxide nanoparticle.
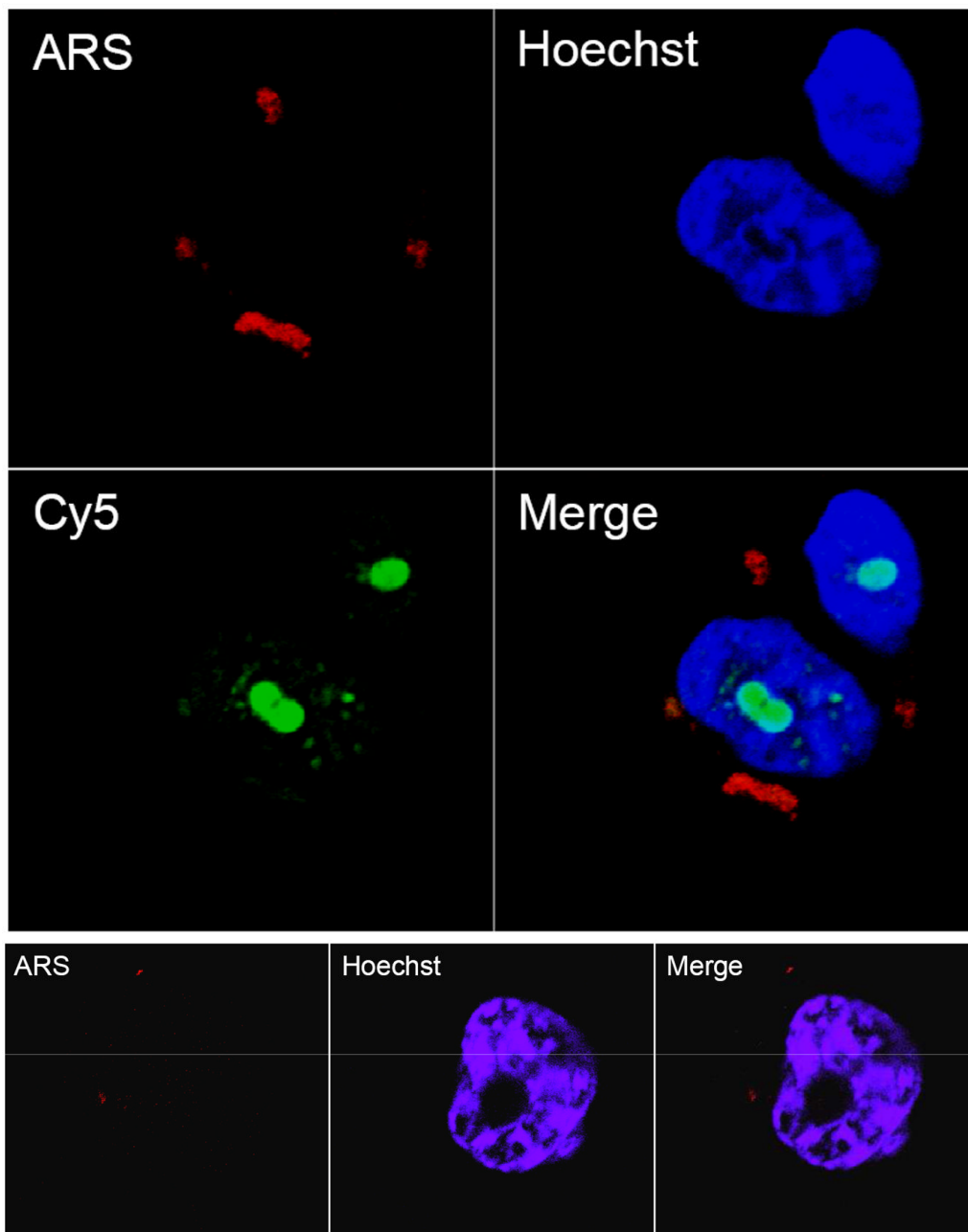
Figure 5.
A. Localization of TiO$_2$ Nanoparticle uptake versus free unbound ODN in PC3M cells. Serum starved cells were treated for 1 hr. with 333 μM of ARS coated TiO$_2$ nanoparticles and with 160 μM of free unbound Cy5 labeled ODN to determine the subcellular localization of each component separately. Results show that the nanoparticles themselves accumulate within endosomal/lysosomal vesicles in the cytoplasm while the ODNs localize with the nucleus and nucleoli.
B. Labeling Intracellular TiO$_2$ in fixed cells. PC3-M cells were treated with unlabeled TiO$_2$ and washed as described above. After fixing in 4% paraformaldehyde, cells were treated with 0.9 mM ARS in PBS for 30 minutes to label the already internalized nanoparticles. Results

showed that internalization of TiO_2 is not dependent on ARS surface modification, and that it is possible to label intracellular nanoparticles in fixed cells.
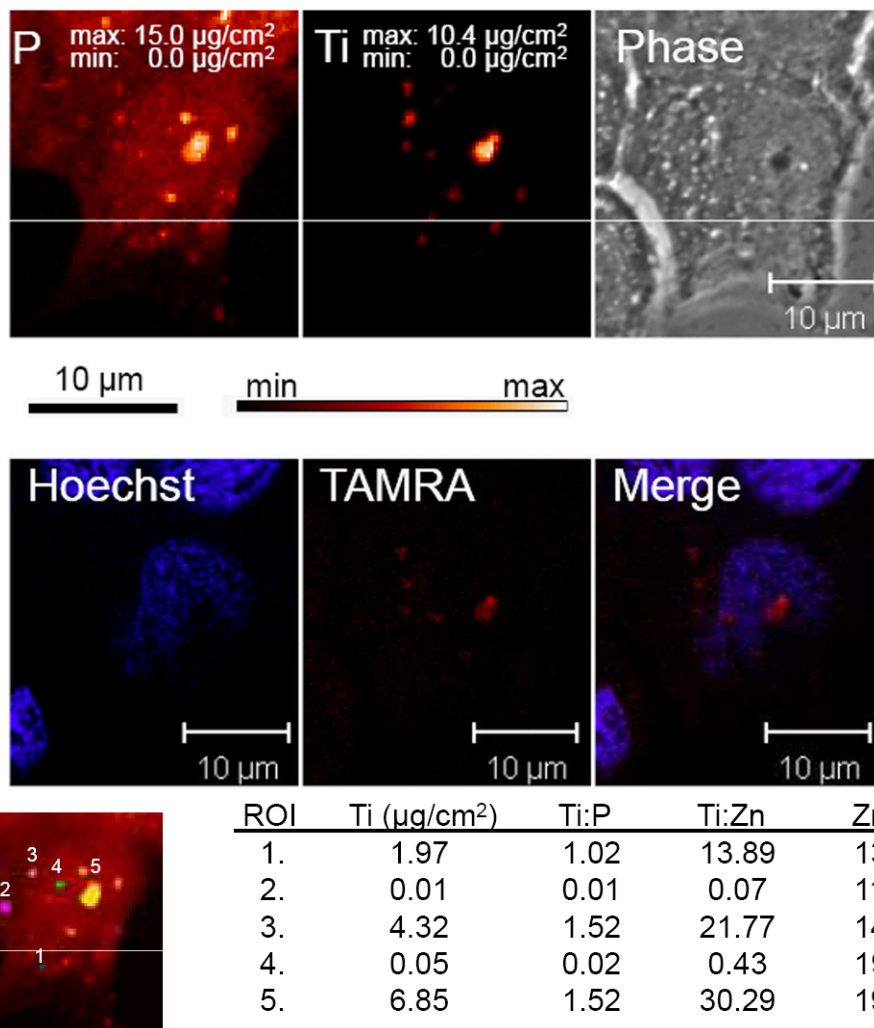
ROI	Ti (μg/cm²)	Ti:P	Ti:Zn	Zn:P
1.	1.97	1.02	13.89	13.58
2.	0.01	0.01	0.07	11.02
3.	4.32	1.52	21.77	14.32
4.	0.05	0.02	0.43	19.47
5.	6.85	1.52	30.29	19.98

Figure 6. Combining X-Ray Fluorescence Microscopy and Fluorescent Confocal Microscopy
A. Combined Use of XFM and fluorescent microscopy to determine relative Nanoconjugate Stability. Breast cancer MCF-7 cells were transfected with 333 μM of TAMRA labeled TiO_2-DNA nanoconjugates, sorted by FACS, seeded on formvar coated EM grids, and allowed to adhere. Next, cells were placed in anti-fade mounting medium and visualized by fluorescent confocal microscopy for the presence of Hoechst and TAMRA. Following microscopy, the EM grids were washed in PBS, and dehydrated in 100% ethanol. Finally same cells were located and analyzed at the 2-ID-D beamline at the Advanced Photon Source at Argonne National Laboratories for the location and concentration of elements from phoshorus to zinc on the periodic table. Top left/center are the images of phosphorus (P) and titanium (Ti) obtained by XRF. Black bar= 10 um for XFM images while white bar= 10 um for confocal images.
B. Quantitative Analysis of Regions of Interest (ROI). Several regions of interest were further analyzed to quantify levels of titanium. Regions 1-3 are cytoplasmic locations, while 4-5 overlap with the nucleus. There was a strong detectable titanium signal in ROIs 1,3, and 5. The ratio of titanium to phosphorus suggests that there is an increase in titanium levels since the Zn:P ratio is consistent within all ROIs.